ELSEVIER

Journal of Computational and Applied Mathematics 108 (1999) 75–86

JOURNAL OF COMPUTATIONAL AND APPLIED MATHEMATICS

www.elsevier.nl/locate/cam

A high-order adaptive numerical method for recirculating flows at large Reynolds number

Sun-Chul Kim[a,1,*], June-Yub Lee[b,c,2]

[a] *Department of Mathematics, Chung-Ang University, Seoul 156-756, South Korea*
[b] *Department of Mathematics, Ewha Womans University, Seoul 120-750, South Korea*
[c] *Korea Institute of Advanced Study, Seoul 136-791, South Korea*

Received 8 September 1998; received in revised form 25 March 1999

Abstract

A numerical method is constructed for two-dimensional Navier–Stokes flows in a circular domain. Adaptive computational grids are employed to resolve the boundary layer and the boundary vorticity values are obtained in high order of accuracy. Numerical results show a quite good agreement with the asymptotic expansion calculation (Kim, SIAM J. Appl. Math. 58(5) (1998) 1394–1413). Extension to general shape domains is briefly addressed.

Keywords: Adaptive method; Navier–Stokes equation; Stream function; Vorticity

1. Introduction

Developing efficient and accurate numerical schemes for given partial differential equations arising in various natural phenomena has been a fascinating topic in mathematics for decades and such methods are gaining importance as tools to analyze many complex physical systems. On the other hand, in spite of huge efforts, the Navier–Stokes equations describing the motion of incompressible viscous fluid still remains an adventurous topic for mathematicians, physicists, and engineers. In particular, only very little is known about the behavior of the solutions as Reynolds number becomes indefinitely large [5]. This corresponds to a singular perturbation problem in partial differential equation which is quite hard to analyze and to compute. Although much effort has been made to understand

* Corresponding author.
E-mail address: kimsc@cau.ac.kr (S.-C. Kim)

[1] The author was supported by the Chung-Ang University Special Research Grants in 1999.
[2] The author was supported by Korea Science and Engineering Foundation, 970701-01013.

0377-0427/99/$ - see front matter
PII: S0377-0427(99)00101-6

the results of large Reynolds number flows, it still remains one of the most challenging research topics in applied mathematics.

If, however, we consider only plane flows, the Navier–Stokes equations can be rewritten as a system of two scalar partial differential equations which are coupled, time dependent and mainly consist of Laplace and convection operators described in Section 2. In terms of this formulation, Prandtl [10] and Batchelor [1] has proposed a theorem: For two-dimensional nested closed streamline flows, the inviscid limit of the solution has constant vorticity with a possible discontinuity on the boundary which is called vortex sheet. For the simplest realization, that is, the flow inside a two-dimensional circular domain, the inviscid limit is calculated asymptotically by applying matching to the outer and inner expansions [5]. This analytic value will be compared to numerical results to test the accuracy of the proposed method in Section 4.

These observations propelled us to start the current research in which we solve large Reynolds number flow using a fast numerical solver for a system of coupled Poisson equations. A Poisson solver for such coupled equations first has to handle an adaptive grid to resolve thin boundary layer properly. In addition, it is required to generate highly accurate derivatives of the solution to obtain the vorticity value on the boundary which can be represented by some combination of the first and the second derivatives of streamline function. Regarding this, we remark that traditional approaches utilize first- or second-order accurate formulas for the boundary vorticity value. (See at [2] for more details.) Once the solution and its derivatives of the equations on an adaptive grid are obtained, iterative schemes described in Section 3 can provide a boundary vorticity value in the desired accuracy thus the solution of the coupled equations. Here, our major concern is the steady state of the flow and for this purpose we used implicit methods in time.

Among many achievements for fast accurate adaptive Poission solvers, Lee and Greengard [7] recently devised a stiff ODE solver which produces the first and the second derivatives of arbitrary-order accuracy as well as the solution itself. Using FFT technique, it is possible to solve the Poisson problem on a disk with thin boundary layer in optimal computational time $O(N)$ where N is the number of grid points. Even though we use in this paper only an arbitrary-order accurate numerical scheme for circular flows using the solver by Lee–Greengard, the method can be extended to any two-dimensional viscous flow problems using a fast adaptive high-order Poisson solver by Greengard and Lee [4]. The two-dimensional solver also provides the solution and the derivatives of arbitrary order accuracy on an adaptive quad-tree domain in optimal computational time $O(N)$. Possible extensions for general two-dimensional domains and related difficulties are briefly discussed in the concluding Section 5.

2. Preliminaries

Presently we are concerned with the incompressible Navier–Stokes equations in non-dimensional form,

$$\nabla \cdot \boldsymbol{u} = 0, \tag{1}$$

$$\frac{\partial \boldsymbol{u}}{\partial t} + \boldsymbol{u} \cdot \nabla \boldsymbol{u} + \nabla p = \frac{1}{\mathrm{Re}} \nabla^2 \boldsymbol{u}, \tag{2}$$

where $\boldsymbol{u} = (u, v, w) \in R^3$ is the velocity vector, p is the pressure, and the positive real parameter Re is the Reynolds number. Another equivalent expression of (2) is found by taking the curl to it,

$$\frac{\partial \Omega}{\partial t} + \boldsymbol{u} \cdot \nabla \Omega = \frac{1}{\mathrm{Re}} \nabla^2 \Omega \tag{3}$$

and is called the vorticity equation where $\Omega = \nabla \times \boldsymbol{u}$ is the vorticity measuring the degree of local rotation.

For two-dimensional flows in which $w = 0$, we introduce the stream function ψ from (1) by

$$\boldsymbol{u} = (u, v) = (\psi_y, -\psi_x) \tag{4}$$

and obtain streamfunction-vorticity formulation of the Navier–Stokes equations

$$\nabla^2 \psi = -\omega, \tag{5}$$

$$\frac{\partial \omega}{\partial t} + \boldsymbol{u} \cdot \nabla \omega = \frac{1}{\mathrm{Re}} \nabla^2 \omega, \tag{6}$$

where ω is the z-component of the vorticity. This formulation has an advantage that we just need to solve two scalar coupled partial differential equations for ψ and $\omega = -\nabla^2 \psi$. Let $D \subset R^2$ be a simply connected domain with sufficiently smooth boundary ∂D. Suppose the streamfunction ψ and the vorticity ω along the boundary ∂D are given simultaneously, then one can simply solve two de-coupled equations, that is, the vorticity in (6) and then the streamfunction in (5) in turn.

In many cases, however, more realistic boundary condition gives only the velocity along the boundary in the form of

$$\boldsymbol{u}(z(s)) = 0\boldsymbol{n} + g(s)\boldsymbol{t},$$

where $\boldsymbol{n}, \boldsymbol{t}$ are normal and tangential vectors to the boundary, respectively and $z(s)$ is a parameterization of the boundary curve. Then the corresponding boundary conditions of (5), (6) are

$$\psi(z(s)) = 0, \qquad \frac{\partial \psi}{\partial n}(z(s)) = -g(s). \tag{7}$$

This set of conditions is too restrictive for ψ and gives no boundary condition for ω, therefore, we have to create a consistent boundary condition for ω. Several approaches have been tried to resolve this vorticity boundary condition. First- or second-order accurate methods based on the neighboring vorticity values and their extrapolation are the simplest-type devices and have been used frequently. Higher-order schemes are possible but produce a problem of stability and hence are not used widely. Formulas of this category are reviewed in unified point of view by E and Liu recently [2]. Another approach utilizing the Green's function is also developed and examined by Wu and Wahbah [12]. This is applied in solving an integral equation to obtain boundary vorticity value.

Here, motivated by the fact that the vorticity is expressed by the second derivative of the stream function, we apply a fast high-order ordinary differential equation solver to obtain an arbitrary-order accurate boundary condition for the vorticity and hence an arbitrary-order accurate method for solving Navier–Stokes flows. The corresponding ordinary differential equations solver is an adaptive solver and thus completely resolves a boundary layer region as we put sufficient points there.

3. A numerical method

For simplicity, we here develop a solver for the steady-state flows in the interior of a unit disk in two dimensions. From the geometry, we introduce the polar coordinate (r,θ) and subsequently

$$u_r = \frac{1}{r}\frac{\partial\psi}{\partial\theta}, \qquad u_\theta = -\frac{\partial\psi}{\partial r} \tag{8}$$

are the velocity components in r,θ directions, respectively. Then (5), (6) become

$$\frac{\partial^2\psi}{\partial r^2} + \frac{1}{r}\frac{\partial\psi}{\partial r} + \frac{1}{r^2}\frac{\partial^2\psi}{\partial\theta^2} = -\omega, \tag{9}$$

$$\frac{\partial^2\omega}{\partial r^2} + \frac{1}{r}\frac{\partial\omega}{\partial r} + \frac{1}{r^2}\frac{\partial^2\omega}{\partial\theta^2} = \frac{\mathrm{Re}}{r}\left(\frac{\partial\psi}{\partial\theta}\frac{\partial\omega}{\partial r} - \frac{\partial\psi}{\partial r}\frac{\partial\omega}{\partial\theta}\right) \tag{10}$$

with the physical boundary condition $(u_r, u_\theta) = (0, g(\theta))$ along the circle. Then the corresponding boundary conditions become

$$\psi(1,\theta) = 0, \qquad \omega(1,\theta) = g(\theta) - \frac{\partial^2\psi}{\partial r^2}(1,\theta) - \frac{\partial^2\psi}{\partial\theta^2}(1,\theta). \tag{11}$$

Note that the second boundary condition for ω is coupled with ψ so we need an iterative scheme to make sure the boundary conditions are satisfied simultaneously.

For fast high-order numerical computation, we further expand ψ, ω in the Fourier-mode form,

$$\psi(r,\theta) = \sum_{n=-N}^{N} \psi_n(r)\mathrm{e}^{\mathrm{i}n\theta}, \qquad \omega(r,\theta) = \sum_{n=-N}^{N} \omega_n(r)\mathrm{e}^{\mathrm{i}n\theta} \tag{12}$$

and obtain the relation

$$\psi_k'' + \frac{1}{r}\psi_k' - \frac{k^2}{r^2}\psi_k = -\omega_k, \tag{13}$$

$$\omega_k'' + \frac{1}{r}\omega_k' - \frac{k^2}{r^2}\omega_k = \frac{\mathrm{Re}}{r}\sum_{l+m=k} \mathrm{i}l(\psi_l\omega_m' - \psi_m'\omega_l) \tag{14}$$

for each mode $k = 0, 1, \ldots, N$. Subsequent boundary conditions are

$$\psi_k(1) = 0, \quad k = 0, 1, 2, \ldots, N \tag{15}$$

from the given physical settings and

$$\psi_0'(0) = 0, \quad \psi_k(0) = 0, \ \ k = 1, 2, \ldots, N \tag{16}$$

from the polar coordinates conditions, respectively. Additionally, from the tangential components of the boundary velocity $g(\theta)$, we have an over-imposed boundary condition on ψ_k

$$g(\theta) = -\sum_{k=0}^{N} \psi_k'(1)\mathrm{e}^{\mathrm{i}k\theta}. \tag{17}$$

We first implement an explicit iterative scheme on these coupled Poisson Eqs. (13), (14) where ψ_k are updated from the previous ω_k for all $k = 1, \ldots, N$ along with boundary condition (15) and

then ω_k are updated using the updated $\psi_{i=0,\ldots,N}$, $\omega_{i=0,\ldots,k-1}$, and the previous $\omega_{i=k,\ldots,N}$. Here boundary value of ω_k are given using the McLaurin-type condition:

$$\omega = -\nabla^2\psi + c\left[\frac{\partial\psi}{\partial n} - g\right] \quad \text{on } \{(r,\theta)\colon r = 1\} \tag{18}$$

which guarantees the convergence if the positive constant c is twice smaller than the smallest eigenvalue of the Laplacian operator [8]. We set $c = 1$ for current computations. Then the resulting equations are two sets of system of Bessel-like second-order differential equations (13), (14) with two proper boundary conditions at $r = 0$ and 1.

There are many numerical methods for solving this standard second-order ordinary differential equations. Multiple shooting, finite difference, and collocation methods are some of the well-known tools, however, we use a fast adaptive integral equation method [7] which first transforms the second-order ordinary differential equation of form

$$u''(r) + p(r)u'(r) + q(r)u(r) = f(r)$$

into an integral equation for $\sigma(r) = u''(r)$:

$$\sigma(r) + p(r)\int_0^1 \frac{\partial}{\partial r}G_0(r,t)\sigma(t)\,\mathrm{d}t + q(r)\int_0^1 G_0(r,t)\sigma(t)\,\mathrm{d}t = f(r)$$

using a piecewise linear Green's function $G_0(r,t)$ satisfying $(\partial^2/\partial t^2)G_0(r,t) = \delta(r-t)$ given homogeneous boundary conditions. The transformation enables us to obtain arbitrary order of accuracy not just for the solution but also for its derivatives up to second order on an adaptive grid. However, high-order discretization of the integral equation generates a dense matrix which is hard to solve by any traditional method in linear computational time. The method in [7] utilizes a fast algorithm to solve the dense matrix in linear computational speed while preserving such good properties as high order of accuracy and adaptivity of grid. Readers may find details about more computational properties in the paper by Lee and Greengard.

Once an iterative solution of the system of ordinary differential equations (13) and (14) with McLaurin-type condition (18) reaches a consistent stage, the order of accuracy of the solution using the consistent boundary condition (11) solely depends on the order of accuracy of $\nabla^2\psi$ and $\partial\psi/\partial n$. Therefore, we obtain the same order of accuracy for computational results as that of the integral equation solver.

The Stokes iteration with an explicit convection term converges fairly well for $\mathrm{Re} < 10$. However, the number of iteration increases as the Reynolds number becomes larger and the numerical solution finally blows up when $\mathrm{Re} > 30$ due to the right hand side convection term in (14). To overcome this phenomenon, we instead consider a time-dependent problem (5), (6) and realize a steady state after a sufficient period of elapsed time. In principle, this corresponds to adding a proper damping term to both sides of Eq. (14).

Since we are mainly concerned with the final steady state, the order of accuracy of a time integrator is not important. We use an implicit scheme such as first-order backward Euler (BE) method or second-order Crank–Nicolson (CN) method for a time integrator instead of explicit Euler method which has time step instability problems due to the diffusive nature of the Navier–Stokes equation. For the BE case Eq. (14) becomes

$$\nabla^2\omega^{\mathrm{n}} - \frac{\mathrm{Re}}{\Delta t}\omega^{\mathrm{n}} = f^{\mathrm{p}} - \frac{\mathrm{Re}}{\Delta t}\omega^{\mathrm{p}}, \tag{19}$$

where f denotes the convection term, the superscript p the previous step, and the superscript n the next step. Thus we incorporate the convection term explicitly again. From proper dimensional analysis, we were able to predict a maximum time step of order $\mathrm{Re}^{-0.5}$ theoretically. This is confirmed by real numerical tests. Similarly for the CN method, we derive

$$\nabla^2\omega^{\mathrm{n}} - 2\frac{\mathrm{Re}}{\Delta t}\omega^{\mathrm{n}} = 2f^{\mathrm{p}} - 2\nabla^2\omega^{\mathrm{p}} - \frac{\mathrm{Re}}{\Delta t}\omega^{\mathrm{p}}. \tag{20}$$

For large Reynolds numbers, we utilize a continuation procedure. We begin to compute the solution with a relatively small Reynolds number and we increase the Reynolds number after arriving at a steady state to achieve another steady state and so on.

4. Numerical results and discussion

4.1. Code validation using an analytic solution

First, we validate our code by comparing the numerical computation with an analytic solution. As long as the authors knowledge goes, we are unaware of any simple exact solution to test the current circular domain problem. Thus we prescribe a stream function in the analytic form

$$\psi(r,\theta) = -\frac{r^2-1}{2}(1+\varepsilon r^4\sin\theta) \tag{21}$$

and Eqs. (5), (6) are modified with a proper source term $h = \frac{5}{2}\varepsilon r^2[\varepsilon r^2(7r^4 - 6r^2 + 3)\sin\theta + 7r^2 - 3]\cos\theta - (1/\mathrm{Re})\frac{15}{2}\varepsilon[35r^2 - 3]\sin\theta$,

$$\nabla^2\psi = -\omega, \tag{22}$$

$$\boldsymbol{u}\cdot\nabla\omega = \frac{1}{\mathrm{Re}}\nabla^2\omega + h, \tag{23}$$

where the parameter $\varepsilon=0$ corresponds to solid body rotation with $\omega=1$. By comparing the numerical and the analytical solution, we are able to confirm that the solver provides high order of accuracy solution on adaptive grid in optimal computation time.

4.2. Numerical computation

Starting with the solid body rotation of the unit disk,

$$\psi(r,\theta) = -\frac{r^2-1}{2}, \qquad \omega(r,\theta) = 1, \tag{24}$$

we impose the perturbed velocity on the boundary,

$$g(\theta) = 1 + \varepsilon\sin\theta. \tag{25}$$

If $\varepsilon \neq 0$, an initial strong discontinuity is inevitable near the boundary whose effect gradually disperses and propagates into the whole region until an equilibrium steady state is achieved. For sufficiently small ε, say 0.2, the final steady state is really the one given by Prandtl and Batchelor [10,1].

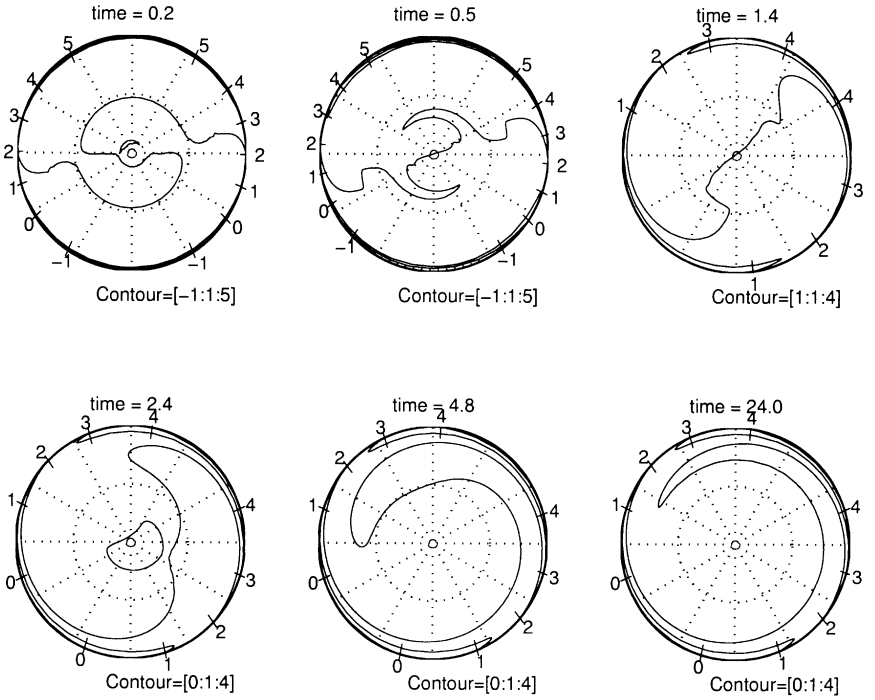

Fig. 1. *Equivorticity lines at* $\mathrm{Re} = 500$ at *different time steps.* Three numbers at the lower right corner show the contour values: start, step, and end value, respectively.

We perform four experiments for discussion. Firstly, we investigate the flow evolution in time and the vorticity profiles at the final steady states in Experiment 1. Secondly, for several large Reynolds numbers, we compute the steady-state solutions using adaptive grids in Experiment 2. Thirdly, constant vorticity values are obtained in and compared with other numerical and asymptotic results from Experiment 3. Lastly, we briefly study large perturbed flows and observe the emerging of a new eddy in Experment 4.

Experiment 1. (*Vorticity profiles for various Reynolds numbers*)**.** We present the flow evolution of $\mathrm{Re} = 500$ at several different times in Fig. 1.

As time elapses, the solution reaches steady-state solution and the vorticity becomes almost constant in a certain concentric circular region and changes catastrophically near the boundary. We monitor the difference of stream function ψ to determine the steadiness in the iterative procedure defined in (19) or (20). The relative update error in the L_2 norm is computed at every 50 time steps until it becomes less than 10^{-4}.

To understand the nature of core vorticity, we have drawn a vorticity profile of various Re along the radial direction in Fig. 2. Here we average out the vorticity on the concentric circle of the corresponding radius. This result for fixed $\varepsilon = 0.2$ clearly implies the constant limit of the vorticity in the whole interior region as $\mathrm{Re} \to \infty$. The flow becomes computationally steady after a much longer time as the Reynolds number increases.

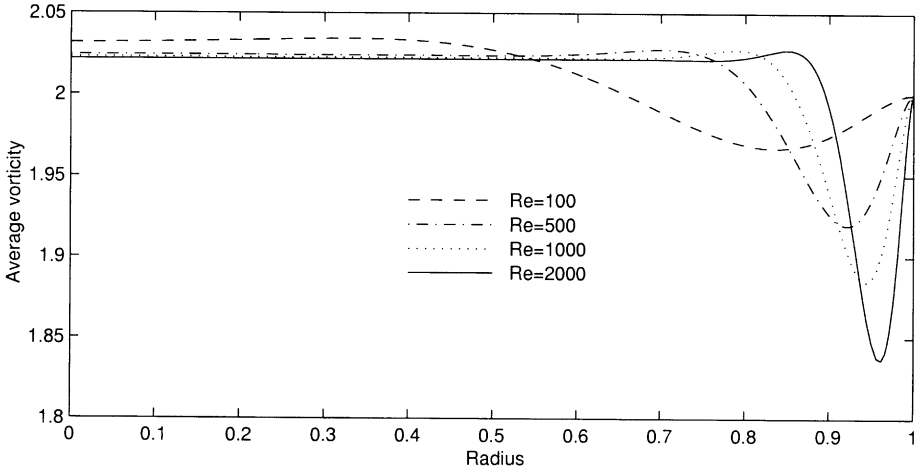

Fig. 2. Vorticity profiles for steady state along r.

Experiment 2. (*Adaptive grids for large Reynolds number flows*)**.** Vorticity profiles along r have been computed for seven different Reynolds numbers, $\mathrm{Re} = 100, 200, 500, 1000, 2000, 5000, 10\,000$. Again we plotted the averaged vorticity values described in Experiment 1. These computations are identical to the previous one, except that our major concern in this experiment is the adaptive meshes which has been automatically generated to resolve the boundary layer using fixed number (we take 16) of subintervals and each of subintervals has eight discretizatoin points. Among seven computed results, only three vorticity profiles at $\mathrm{Re} = 100, 1000, 10\,000$ have been displayed in the figure below. The grids adopted for the seven computations are drawn on the lower plot and the corresponding Reynolds numbers are indicated on the left-hand side plot in Fig. 3.

The mesh used in the computation with $\mathrm{Re} = 100$ is relatively uniform and the ratio of the maximum to the minimum subinterval length is 8. As the Reynolds number becomes larger, the vorticity changes rapidly near the boundary in which more narrow meshes are required to resolve the boundary layer. At $\mathrm{Re} = 10\,000$, the subinterval length near $r = 0$ is $\frac{1}{4}$ while that near $r = 1$ is $\frac{1}{128}$. Thus, the ratio is 32 which enables substantial speed up for computation compared to the corresponding uniform grid. In conclusion, such adaptive mesh becomes essential when the Reynolds number increases indefinitely.

For high Reynolds number flow, azimuthal transition is less dramatic than the formation of thin boundary layer. (See Fig. 1.) To justify the number of Fourier modes N required for four digits of accuracy computation, we perform the same experiments as above for three different Reynolds numbers, $\mathrm{Re} = 100, 1000, 10\,000$. The result in Fig. 4 shows L_2-averages of $\omega_k(r)$ for $k = 1, \ldots, N$

$$\|w\|_2(k) := \frac{\int_0^1 |\omega_k(r)|^2 r \, \mathrm{d}r}{\int_0^1 r \, \mathrm{d}r}.$$

The number of angular frequency modes is not rapidly increasing compared to the number of grid points in radial direction when Reynolds number becomes larger. For Reynolds number 100–1000, eight modes seems to be adequate to obtain four digit accurate solutions, however, we doubled the

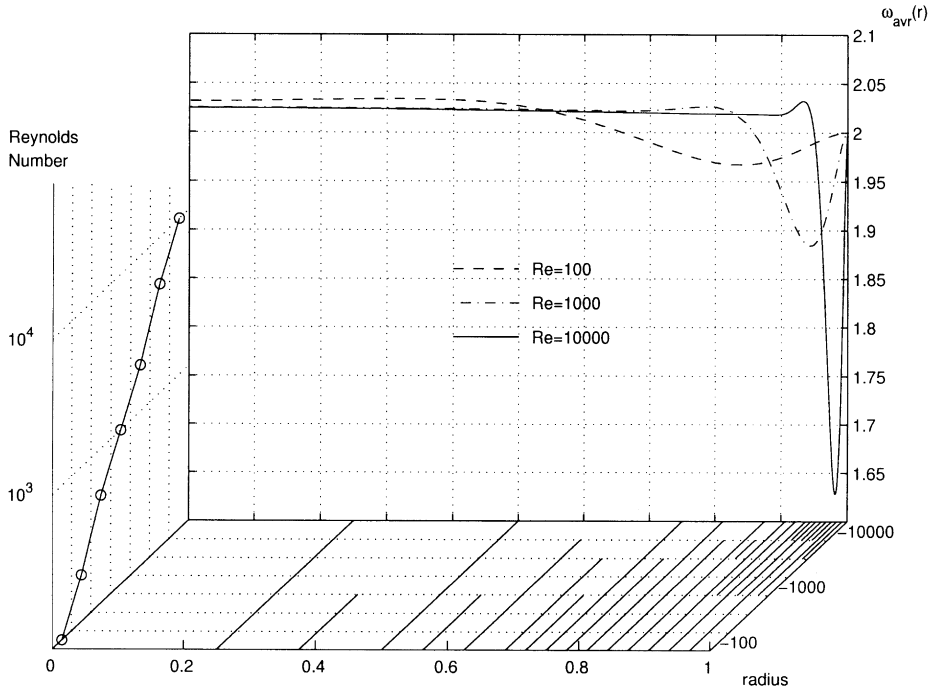

Fig. 3. *Vorticity profiles and adaptive meshes.* Vorticity profiles for $\mathrm{Re} = 100, 1000, 10\,000$ have been drawn on the main plot. The lower plot shows automatically generated adaptive meshes and the left-hand side plot shows the corresponding Reynolds numbers.

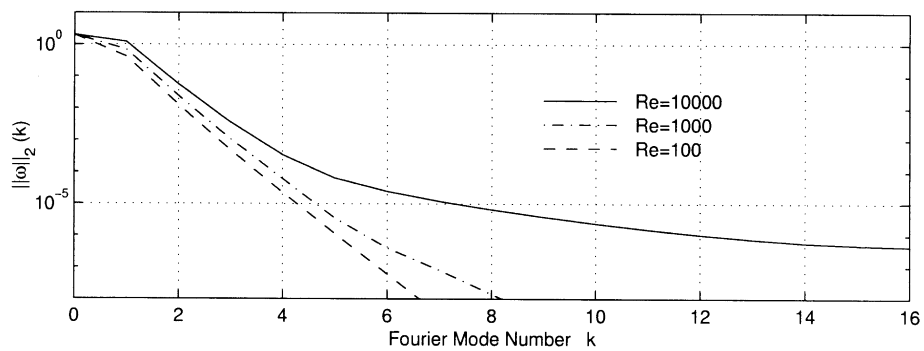

Fig. 4. *Decay of high angular frequency modes.* L_2-average of ω_k, $\|\omega\|_2(k)$ for $k = 1, \ldots, 16$ at $\mathrm{Re} = 100, 1000, 10\,000$.

number of angular modes $N = 16$ to avoid the mode aliasing effect in the nonlinear source term $(1/r)(\psi_\theta \omega_r - \psi_r \omega_\theta)$.

Experiment 3. (*Core vorticity comparison*)**.** The final core vorticity can be computed not just using numerical methods but also asymptotic techniques. The Batchelor–Wood formula is a first-order accurate analytic result and the asymptotic result by Kim [5] using a matched asymptotic expansion

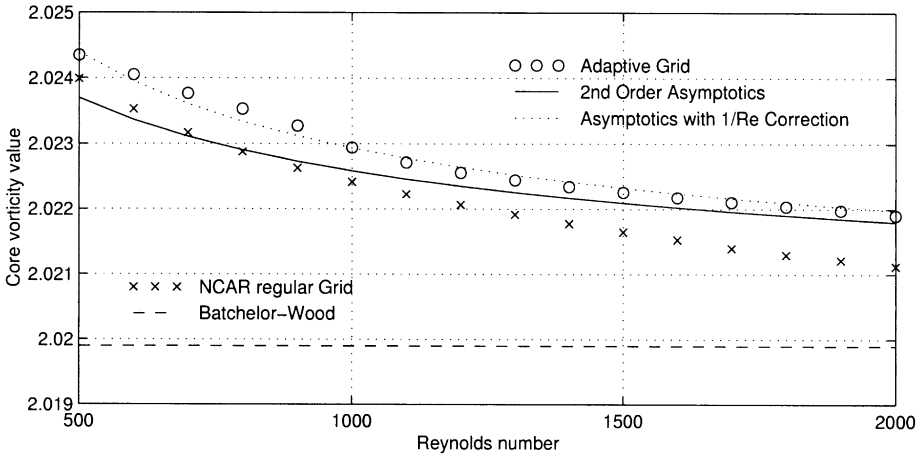

Fig. 5. *Comparison of vorticity values.* Two numerical results are marked with ∘, × and two asymptotic expansion results are shown with solid or dashed lines. Read the text below for the explanation of the dotted line.

has second-order accuracy with respect to the perturbation parameter ε,

$$\omega_{\text{exact}} \approx 2\sqrt{1+\frac{\varepsilon^2}{2}+\frac{3\sqrt{2}}{2\sqrt{\text{Re}}}\varepsilon^2+\text{O}\left(\frac{1}{\text{Re}}\right)}. \tag{26}$$

In this expression, we ignore the exponentially small terms in Re which might be a possible contribution to the total error.

Another numerical result, using a NCAR Poisson solver `hwsplr` with polar-grid regular mesh (200 in the r-direction and 100 in the θ-direction) and Crank–Nicolson method in time stepping, is displayed for comparison [5]. For the boundary vorticity values, Thom's first order formula [2] is used.

During the current computation, we use eighth-order Chebyshev nodes in each of 16 intervals which makes 128 adaptive grid points in r-direction and 32 nodes (or equivalently, $N = 16$ Fourier modes) in θ-direction. For a more accurate result, the code is run until the relative difference of stream function after 50 iteration becomes less than 10^{-6} in L_2 norm to arrive at a constant vorticity limit state.

We compare five different values of the core vorticity in Fig. 5. The dashed line shows the asymptotic result by Batchelor–Wood and a NCAR Poisson solver on a regular grid results are marked with ×. Our computational results are marked with ∘, the solid line displays the second-order matched expansion formula by Kim, and the dotted line indicates the second-order asymptotic results with a correction term O(1/Re) to fit our experiments.

The method, using a NCAR solver on a uniform grid at some higher Reynolds number, shows some unignorable error probably coming from poorly resolved boundary layer. The number of grid points required to resolve the boundary layer using a uniform grid is proportional to the square root of the Reynolds number while the number using our solver with an adaptive grid is nearly constant. Our present method produces quite good agreement with the second-order analytic result. The discrepancy between numerical results and the second-order expansion for $\text{Re} < 1200$ is explained from the limit of validity for the analytic approach which produces asymptotics. To justify our argument, we try

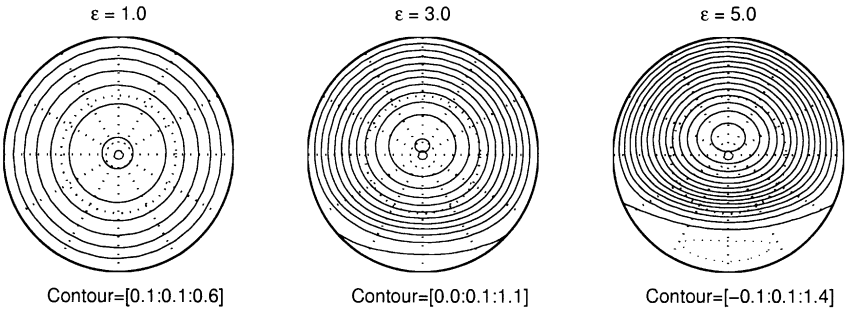

Fig. 6. *Streamlines at* $\mathrm{Re} = 1000$ *with different perturbations.* The contour values are described at the lower right corner as in Fig. 1 and the dotted contour line corresponds to a negative contour value.

to guess numerically the first missing term in the second order expansion and realize that adding a correction term $0.35\,(1/\mathrm{Re})$ makes the expansion in better agreement with our numerical computations for the whole range of Reynolds number, $\mathrm{Re} = 500$–2000.

Experiment 4. (*Large perturbation case*)**.** For the final demonstration, we increase the perturbation and observe that the flow speed becomes negative in some part (near $\theta = \pi$) and eventually has more than one eddy inside. We provide several cases under fixed $\mathrm{Re} = 1000$ in Fig. 6. More precisely, the convergence of boundary layer solution to one-eddy constant vorticity state is proved for $\varepsilon = 0.2$ in [5]. Until some critical ε, we observe one-eddy structure is being kept. For a bigger ε a new opposite eddy emerges in the lower half of the disk. Further study with various boundary data is worthwhile for designing a simple model in high Reynolds number internal flows [6].

5. Final remarks

We obtained a solver for the circular domain which produces separable partial differential equations (9), (10) and there seems no difficulty in extending the method to cover other domains of separable geometry. Furthermore, it is possible to extend the method to the problem in arbitrarily closed domains in the following consideration. The vorticity is represented by the combination of the second- and lower-order derivatives of the stream function in the case of general curvilinear coordinates. Thus the correct vorticity values at the curvilinear boundary can be computed from a generalization of formula (11) to the curvilinear case. In order to accomplish this task, a Poisson solver for a general adaptive domain in R^2 has to provide accurate solutions and its derivatives. Once the derivatives are obtained, then a similar iterative procedure produces an arbitrary high-order solver for any two-dimensional domain.

The Poisson solver by Greengard and Lee [4] is for arbitrary domains and thus we can utilize it for the current purpose. Though the two-dimensional solver provides adaptive solutions of arbitrary order accuracy in the optimal computational timing $\mathrm{O}(N)$, the computational cost for general domain problems is much higher than that for a circular domain. The reason is that the boundary layer in the circular domain is parallel to the $r = 1$ axis in (r, θ) coordinate, however, there is no easy way to resolve the thin boundary layer along the arbitrary boundary curve in R^2 using rectangular adaptive

grids which have been used in the solver by Greengard and Lee [4]. The simplest way to resolve the problem is placing the grid points in the same spacing with the boundary layer of $1/\sqrt{\mathrm{Re}}$ thickness and in such case, the number of grid points required proportionally increases as Re gets bigger.

And other than the difficulty of numerical computation, we have to pay attention to the existence of a steady state. It is not a question in a circular domain since the rigid body rotation in a circular eddy is absolutely stable [5], however, this is not true anymore in general domains. The solution we seek, that is, the constant vorticity flow might not be realized forever in time. In this case the flow might be unstable and the computation is subtle. This is a deferred topic for future research.

6. For further reading

The following references are also of interest to the reader: [3,9,11]

References

[1] G.K. Batchelor, On steady laminar flow with closed streamlines at large Reynolds number, J. Fluid Mech. 1 (1956) 177–190.
[2] W.E. Liu, J.-G. Liu, Vorticity boundary condition and related issues for finite difference schemes, J. Comput. Phys. 124 (1996) 368–382.
[3] L. Greengard, M.C. Kropinski, An integral equation approach to the incompressible Navier–Stokes equations in two dimensions, DOE Technical Report 97-002 Courant Mathematics and Computing Laboratory, 1997.
[4] L. Greengard, J.-Y. Lee, A direct adaptive Poisson solver of arbitrary order accuracy, J. Comput. Phys. 125 (1996) 415–424.
[5] S.-C. Kim, On Prandtl–Batchelor theory of a cylindrical eddy: asymptotic Study, SIAM J. Appl. Math. 58 (5) (1998) 1394–1413.
[6] P.A. Lagerstrom, Solutions of the Navier–Stokes equation at large Reynolds number, SIAM J. Appl. Math. 28 (1) (1975) 202–214.
[7] J.-Y. Lee, L. Greengard, A fast adaptive numerical method for stiff two-point boundary value problems, SIAM Sci. Comput. 18 (2) (1997) 403–429.
[8] Johnnie W. McLaurin, A general coupled equation approach for solving the biharmonic boundary value problem, SIAM J. Numer. Anal. 11 (1) (1974) 14–33.
[9] R. Peyret, T.D. Taylor, Computational Methods for Fluid Flow, Springer, Berlin, 1983.
[10] L. Prandtl, Uber Flussigkeitsbewegung bei sehr kleiner Reibung, International Mathematical Congress, Heidelberg, 1904, pp. 484–491; see Gesammelte Abhandlungen II (1961) 575–584.
[11] R. Schreiber, H.B. Keller, Driven cavity flows by efficient numerical techniques, J. Comput. Phys. 49 (1983) 310–333.
[12] J.C. Wu, M.M. Wahbah, Lecture Notes in Physics, Vol. 59, Springer, New York, 1976, pp. 448–453.